JOURNAL OF MATERIALS SCIENCE 7 (1972) 1299–1307

Improvements in the transverse properties of composites

Part 1 *Fracture surface energy and mechanism of transverse fracture in glass fibre composites*

G. MAROM, E. F. T. WHITE
Department of Polymer and Fibre Science, The University of Manchester Institute of Science and Technology, Manchester, UK

Fracture surface energies of initiation (γ_I^c) for a transverse fracture process in glass-reinforced epoxy composites have been measured and the results calculated by three different treatments and are compared with the average fracture surface energies (γ_F^c) for the complete fracture process.

Changes in these two fracture properties are studied as a function of the volume fraction of the fibres, and the relation between the surface energies is established as a factor which determines the nature of the fracture process. When $\gamma_I^c - \gamma_F^c > 0$ a catastrophic failure is expected, whereas a controlled fracture is observed for $\gamma_I^c - \gamma_F^c < 0$.

1. Introduction

Fracture processes in composite materials require a greater understanding, if these materials are to be used for engineering purposes. Composites to be used at the highest level of properties must necessarily be constructed of highly aligned fibrous reinforcement, and it is this measure of alignment that contributes to their high stiffnesses and strength in the fibre direction. Such reinforcement, however, confers poor stiffness, strength and crack growth resistance to stresses in the transverse direction.

The process of fracture in fibrous composite materials will generally involve an initiation process, in which the crack first develops. This first-formed initial crack may subsequently behave in three possible ways. It may (i) remain stable; (ii) grow in a steady controlled fashion; or (iii) propagate catastrophically leading to immediate rupture of the sample. The relative energies, required for the initiation and continued growth of the first-formed crack, the stress geometry and the material properties determine which of the above processes will occur.

Fracture in a fibre-reinforced composite can include the creation of three types of fracture face, namely: (i) creation of new matrix surface due to growth of the crack through pure matrix zones; (ii) formation of new end-surfaces of fibres due to fibre breakages; (iii) development of new surface of matrix and fibres due to fracture of the interface and subsequent debonding of fibres from the matrix. It should be noted that the energies required to create a new matrix surface by debonding at the interface, may be different from those required to create a matrix failure surface. The latter may involve considerable plastic deformation and consequent high fracture surface energy, whereas failure in the interfacial region need not necessarily involve plastic flow in the matrix. There are several conventional test methods for evaluating the transverse strength of unidirectional composites, for example, by measuring the transverse flexural strength, or by measuring the shear strength [1]. These methods often measure structural properties which are dependent on the type and geometry of specimen, and do not measure a basic parameter that is applicable to all test methods. However, it has been postulated [2] that the fracture surface energy (or the strain-energy release rate) is a bulk property of the material and thus is independent of the specimen configuration. It seems reasonable therefore to use the methods

of fracture mechanics to measure the fracture surface energy as a means of analysing the failure behaviour of composites.

Generally, the fracture surface energy, γ is defined as the work required to create unit area of fracture face, irrespective of the type or types of new surface comprising the fracture face, or of its microscopic shape. A distinction is often made [3] between two values of γ: γ_I, the value of γ used in the Griffith equation [4], and γ_F, the value averaged over the whole fracture process. γ_I is related to the stain–energy release rate at the instant of fracture by $-(\partial U/\partial A) \geqslant \gamma_I$, where A is the area of the new fracture face, whereas γ_F is related to the total energy which is dissipated in the complete fracture process by $\gamma_F = U/A$. For a given material γ_I and γ_F are not necessarily the same.

It is of interest to establish the relation between γ_I and γ_F along the whole range of the volume fraction of the fibres, as this relation governs the nature of the fracture process, that is whether fracture proceeds catastrophically or in a controlled fashion.

2. Specimen preparation and testing

"Araldite" (CIBA Ltd) epoxy resin MY.750, cured by the hardener HT.972 was used as the resin for all specimen preparations. E-glass fibres in the form of 408 strand rovings without surface treatment were used for the reinforcement. Pure resin was cast in a 10 × 10 cm open mould to produce plates of 0.5 cm thickness. Composites were made by close winding the glass rovings at a density of 10 turns per 1 cm width on a winding machine drum (26 cm diameter) to form 10 cm wide strips. These were impregnated with an acetone solution of the resin, cut into 10 × 10 cm flat sheets and moulded in a three plate mould under 100 psi. pressure at 170°C to form 0.5 cm thick sheets. The volume fraction of the fibres was controlled by the number of "pre-preg" sheets introduced into the mould, and by the amount of resin squeezed out in the moulding process. The moulding plates were cut into specimens of the form of 0.5 cm square-section bars, 4.5 cm long. Cuts to a depth of c, equal to multiples of one tenth of the beam thickness, were made at the centre of each bar (Fig. 1a). In specimens of pure matrix a scratch was made at the bottom of the cut, similar to a method described for metals [5] in order to diminish plastic deformation, and to reduce the scatter of the results. In the composites the fibre direction was as indicated in Fig. 1b. The specimens were tested in three-point bending on an Instron machine at crosshead speed of 0.05 cm/min. Typical load-deflection curves are shown in Fig. 2.

3. Transverse strength

Cooper and Kelly [6] and Gerberich [7] suggest that in the case of no interfacial contribution Equation 1 applies:

$$\sigma_t^c = \sigma_m[1 - \sqrt{(4V_f/\pi)}] \quad (1)$$

where σ_t^c is the transverse strength of the composite, σ_m is the strength of the matrix and V_f is the volume fraction of the fibres. This function is shown in Fig. 3 for $\sigma_m = 120$ MN/m². Equation 1 was developed for the case of fibres being packed in a square array in the resin, σ_t^c becomes zero for $V_f = 0.79$ – a situation in which the fibres would be in contact throughout. For fibre-matrix interfacial strength greater than zero the "law of mixtures" is applied giving the following result.

$$\sigma_t^c = \sigma_m[1 - \sqrt{(4V_f/\pi)}] + \sigma_i\sqrt{(4V_f/\pi)} \quad (2)$$

where σ_i is the tensile stress necessary to separate

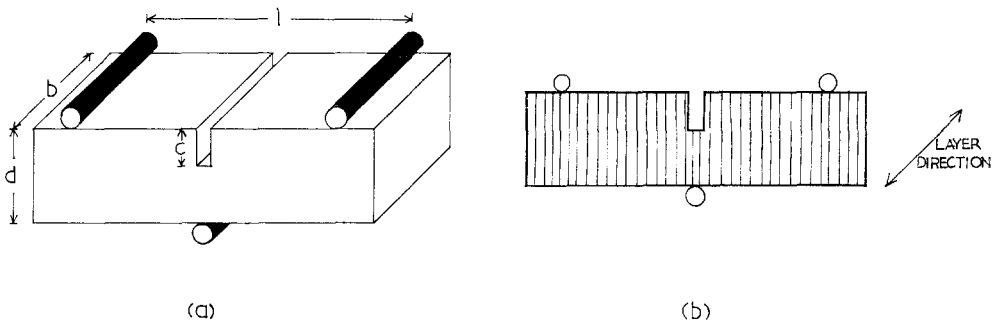

Figure 1 (a) The specimen geometry. (b) The fibre direction in regard to the specimen geometry and the mode of loading.

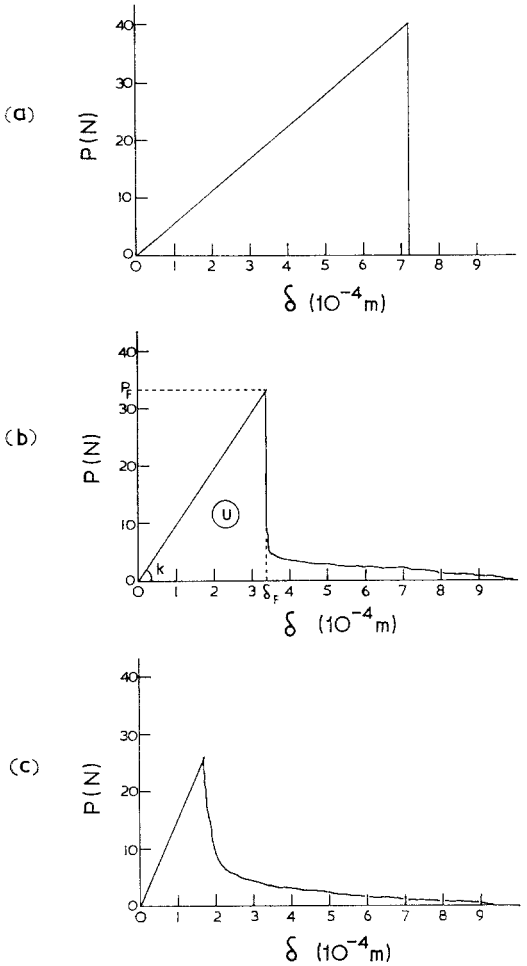

Figure 2 Typical load-deflection curves for specimens of $c/d = 0.4$, indicating load and deflection at fracture and total fracture energy. (a) Pure matrix; (b) Composite, $V_f = 0.27$; (c) Composite, $V_f = 0.45$.

the fibre from the matrix under transverse loading.

Similarly, it is possible to develop an equation for the case of hexagonal array of the fibres in the matrix arranged as in Fig. 4. Here we assume the crack grows in the matrix by the shortest path [2, 8]. For hexagonal arrangement of the fibres in the matrix the inter-fibre spacing, λ, and the centre-to-centre fibre spacing, λ', are given in terms of the fibre radius, r, and V_f by the following equations:

$$\lambda' = 2r\sqrt{[\pi/2\sqrt{3}V_f)]},\ \lambda = 2r\sqrt{[\pi/(2\sqrt{3}V_f)]} - 2r \quad (3)$$

When the fibre-matrix interfacial strength is zero, the transverse strength is reduced by the

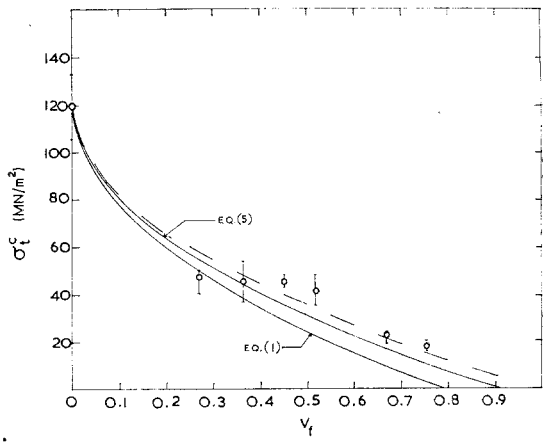

Figure 3 Transverse flexural strength of the composites as a function of the volume fraction. A comparison of experimental results with various theoretical expressions.

ratio $A_m/A = \lambda/\lambda'$, where A_m is the matrix area and A_m/A is the matrix area fraction.

$$\lambda/\lambda' = 1 - \sqrt{[(2\sqrt{3}V_f)/\pi]} \quad (4)$$

Hence:

$$\sigma_t^c = \sigma_m\{1 - \sqrt{[(2\sqrt{3}V_f)/\pi]}\} \quad (5)$$

Equation 5 is shown plotted in Fig. 3. Now, σ_t^c becomes zero at $V_f = 0.906$ (close hexagonal array).

For fibre-matrix interfacial strength greater than zero the "law of mixtures" may be applied giving the following:

$$\sigma_t^c = \sigma_m\{1 - \sqrt{[(2\sqrt{3}V_f)/\pi]}\} + \sigma_i\sqrt{[(2\sqrt{3}V_f)/\pi]} \quad (6)$$

σ_t^c values for samples tested in bending experiments are shown in Fig. 3. Substitution of the experimental results into Equation 6 gave an average value for σ_i of 5 MN/m².

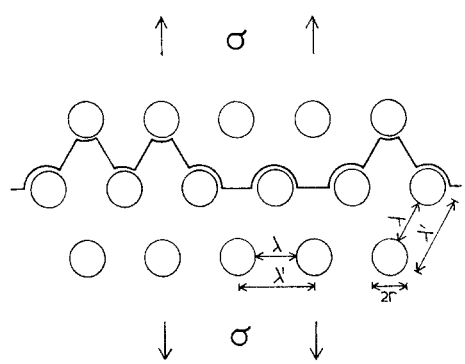

Figure 4 A schematic transverse fracture path in a composite of hexagonal array fractured in a bending mode.

4. Fracture surface energy of initiation

4.1. Determination of γ_I

Various approximations can be used for calculating the γ_I values from the experimental results. Three of these methods were used in this work, and the results were compared.

The first approximation is the compliance method [9, 10]. It is based on the fact that at the instant of fracture initiation $\gamma_I = -(\partial U/\partial A)_\delta$ where A is the total area of the cut. Taking $U = P_F\delta_F/2 = k\,\delta_F^2/2$ and $(\partial U/\partial k) = \delta_F^2/2$ it can be shown that

$$\gamma_{I_1} = -\frac{\delta_F^2}{2}\frac{\partial k}{\partial A} \tag{7}$$

k and δ are described in Fig. 2.

The term $\partial k/\partial A$ can be determined experimentally by measuring the stiffness of specimens, containing a range of crack areas, and then measuring the appropriate slope of a plot of k as a function of A. It is important to note that this approximation does not consider the shape or the geometry of the specimen, or the change from plane-strain to plane-stress conditions with increasing c/d ratio.

The second approximation is based on stress intensity factor (K_I) calibrations [11–13]. The term K_I describes the external loading and the geometries of the crack and of the specimen, it has been shown by Irwin [14] that γ_I and K_I are related by $K_I^2 = 2E\gamma_I$, where E is the transverse Young's modulus of the composite. K_I is often expressed by a geometrical term, Y, which is c/d dependent. For three-point bending specimens $Y = K_I bd^2/6Mc^{\frac{1}{2}}$, where M is the applied bending moment which for a rectangular bar is $M = \sigma_F bd^2/6$, and $\sigma_F = 3P_F l/2bd^2$ is the fracture stress. Hence

$$\gamma_{I_2} = \frac{Y^2\,\sigma_F^2\,c}{2E} \tag{8}$$

Brown and Srawley [11] expressed Y to within 0.2% by fourth-degree polynomials of the form

$$Y = A_0 + A_1(c/d) + A_2(c/d)^2 + A_3(c/d)^3 + A_4(c/d)^4.$$

For $l/d = 8$, A has the following values: $A_0 = +1.96$, $A_1 = -2.75$, $A_2 = +13.66$, $A_3 = -23.98$, $A_4 = +25.22$. The calculated values of Y used in this work are shown in Table I.

The third approximation is based on applying a correction to the Griffith equation for plane-strain conditions, i.e. $\gamma_I = (1-\nu^2)\,\pi\,\sigma_F^2 c/2E$ where ν is the appropriate Poisson's ratio. Such a correction will allow for a wider range of c/d, i.e. plane stress as well as plane strain conditions. For convenience, the corrected Griffith equation is often [5, 15] presented in the form:

$$\gamma_{I_3} = \frac{9\,(1-\nu^2)P_F^2 l^2}{8Eb^2(d-c)^3}\,f\left(\frac{c}{d}\right) \tag{9}$$

where $f(c/d)$ is a dimensionless function of c/d. At small c/d values $f(c/d) = \pi\,c(d-c)^3/d^4$, and the equation reduces to the original Griffith equation. The values of $f(c/d)$ were calculated by various mathematical treatments. Table I shows the results of one of these treatments [3] made for four-point-bending specimens.

TABLE I Values of $f(c/d)$ and of Y as a function of c/d

c/d	0.1	0.2	0.3	0.4	0.5	0.6
$f(c/d)$	0.23	0.36	0.41	0.43	0.43	0.43
Y	1.80	1.81	1.93	2.16	2.58	3.32

All three approximations described above were used for determining γ_I^c from the experimental results. The values of $f(c/d)$ used in the calculation, were the values for four-point-bending specimens, shown in Table I, with an error of less than 10% [5]. The factor $(1-\nu^2)$ which is an approximation [5] was taken to equal 1. The transverse Young's moduli for all samples were determined by three-point-bending tests of the un-notched beams, using the equation $E = k\,l^3/4bd^3$ (ASTM D.790). The experimental results for the appropriate modulus E are shown in Fig. 5. The results for γ_I^c from these results are summarized in Table II. As mentioned previously in Section 2 the results for the pure matrix were highly dependent on the nature of the cut, and the final value of γ_I^m was, therefore, determined from the average of three sets of results, with a scatter of ~40%. The γ_I^m results in Table II are of one of these sets.

All specimens of pure matrix exhibited catastrophic fracture for every c/d. Un-notched specimens and those containing shallow cuts of composites of $V_f = 0.27$ – in which a relatively high energy was built up before fracture occurred – also failed in a catastrophic fashion, resulting two pieces which were being held together by a few misaligned fibres. The energy

TABLE II γ_I^c values calculated by the compliance method, by K_I calibration method and from the Griffith equation

V_f	0*				0.27				0.37				0.45				0.52				0.67				0.76			
c/d	$\gamma_{I_1}^c$	$\gamma_{I_2}^c$	$\gamma_{I_3}^c$	γ_I^cav	$\gamma_{I_1}^c$	$\gamma_{I_2}^c$	$\gamma_{I_3}^c$	γ_I^cav	$\gamma_{I_1}^c$	$\gamma_{I_2}^c$	$\gamma_{I_3}^c$	γ_I^cav	$\gamma_{I_1}^c$	$\gamma_{I_2}^c$	$\gamma_{I_3}^c$	γ_I^cav	$\gamma_{I_1}^c$	$\gamma_{I_2}^c$	$\gamma_{I_3}^c$	γ_I^cav	$\gamma_{I_1}^c$	$\gamma_{I_2}^c$	$\gamma_{I_3}^c$	γ_I^cav	$\gamma_{I_1}^c$	$\gamma_{I_2}^c$	$\gamma_{I_3}^c$	γ_I^cav
														10^2 J/m^2														
0.1	3.2	4.6	2.4	3.0	2.4	2.3	2.4	2.4	1.9	1.3	1.3	1.6	0.89	0.94	0.92	0.91	0.70	0.77	0.79	0.74	0.26	0.25	0.26	0.26	0.12	0.16	0.15	0.14
0.2	3.0	2.9	3.3	3.1	2.8	3.0	3.2	3.0	1.4	1.4	1.5	1.4	0.85	1.2	1.3	1.1	0.80	1.1	1.2	0.98	0.17	0.32	0.32	0.25	0.15	0.18	0.19	0.17
0.3	4.1	3.8	4.0	4.0	3.4	2.8	3.0	3.2	1.7	1.8	1.8	1.8	1.3	1.4	1.5	1.4	0.93	1.1	1.1	1.0	0.24	0.38	0.44	0.33	0.24	0.17	0.18	0.21
0.4	4.0	3.9	4.5	4.1	3.2	3.1	3.3	3.2	1.8	1.8	1.9	1.8	0.96	1.2	1.3	1.1	0.93	0.99	1.3	1.0	0.32	0.39	0.41	0.36	0.37	0.14	0.15	0.26
0.5	4.9	4.4	4.2	4.6	3.4	3.2	3.2	3.3	1.5	1.4	1.5	1.5	0.96	1.3	1.3	1.1	0.81	1.2	1.1	0.98	0.23	0.28	0.28	0.26	0.24	0.10	0.11	0.18
0.6	5.7	4.8	5.1	5.4	2.6	2.3	2.2	2.4	1.6	1.3	1.4	1.5	0.85	1.0	1.5	1.1	0.70	1.3	1.1	0.95	0.29	0.29	0.27	0.29	0.24	0.12	0.11	0.18
0.7	6.9	—	—	6.9	1.7	—	—	1.7	1.4	—	—	1.4	0.96	—	—	0.96	0.70	—	—	0.70	0.39	—	—	0.39	0.24	—	—	0.24
0.8	3.9	—	—	3.9	1.7	—	—	1.7	0.78	—	—	0.78	0.88	—	—	0.88	0.73	—	—	0.73	0.49	—	—	0.49	0.18	—	—	0.18
0.9	5.9	—	—	5.9	2.2	—	—	2.2	0.50	—	—	0.50	0.69	—	—	0.69	0.66	—	—	0.66	0.15	—	—	0.15	—	—	—	—

*Results for one set of specimens only.

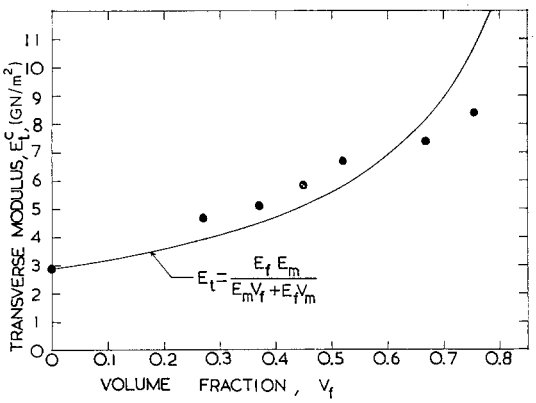

Figure 5 Transverse Young's moduli of the composites as a function of the volume fraction compared with the theoretical lower bound.

required to accomplish the separation of the two pieces was not recorded when using the initial scale sensitivity of the Instron machine. Specimens of the rest of the tested composites for every c/d exhibited controlled fracture. It is obvious that almost similar values of $\gamma_I{}^c$ were obtained by using the second and the third approximations. These values were in very good agreement with the values of $\gamma_I{}^c$ obtained by applying the compliance method to the experimental results. As the compliance method is the only one out of these three, which does not take into account the geometry of the specimens, the final value of $\gamma_I{}^c$ for every c/d was calculated by taking an average $\gamma_I{}^c$ using the following formula:

$$\gamma_I{}^c = [(\gamma_{I_2}{}^c + \gamma_{I_3}{}^c)/2 + \gamma_{I_1}{}^c]/2.$$

In this way, a single value of $\gamma_I{}^c$ for every value of c/d was obtained. The final results show a consistent variation of $\gamma_I{}^c$ as a function of c/d for most of the samples. This variation is illustrated in Fig. 6. Since it is obvious that the results of $\gamma_I{}^c$ for c/d values in the range of $0.2 \leqslant c/d \leqslant 0.6$ are very similar, and as this test has been previously recommended [5, 12] to be carried out for low values of c/d, the average $\gamma_I{}^c$ taken over the range $0.2 \leqslant c/d \leqslant 0.6$ was therefore calculated for every tested V_f to be the surface fracture energy. The results are shown in Fig. 7.

4.2. $\gamma_I{}^c$ as a function of V_f

Gerberich [7] – basing his considerations on the existence of high plastic deformation zones in the immediate vicinity of the fracture, and by calculating the volume of the matrix material involved in plastic energy dissipation – suggests that for a square array of the fibres, and for a zero interfacial area

$$\gamma_I{}^c = 2\,\sigma_m\,\epsilon_m\,r\,[\sqrt{(\pi/4V_f)} - 1] \qquad (10)$$

where σ_m is the nominal fracture stress and ϵ_m is the true fracture strain. A comparison of Equation 10 – substituting $\epsilon_m = \sigma_m/E_m$ and using $\sigma_m = 120$ MN/m^2, $E_m = 2.9$ GN/m^2, and $2r = 15.2 \times 10^{-6}$m (as measured) with the experimental observations is shown in Fig. 7.

A different approach to this problem is to adopt the same considerations used for $\sigma_t{}^c$. Assuming that there is no fibre breakage during the fracture initiation along the fibre direction, only two of the three possible fracture-face types are formed, and therefore, only $\gamma_I{}^m$ and $\gamma_I{}^i$ – the fracture surface energy of initiation of the matrix and interface respectively – will contribute to the final value of $\gamma_I{}^c$. The contribution depends on the proportion of each type

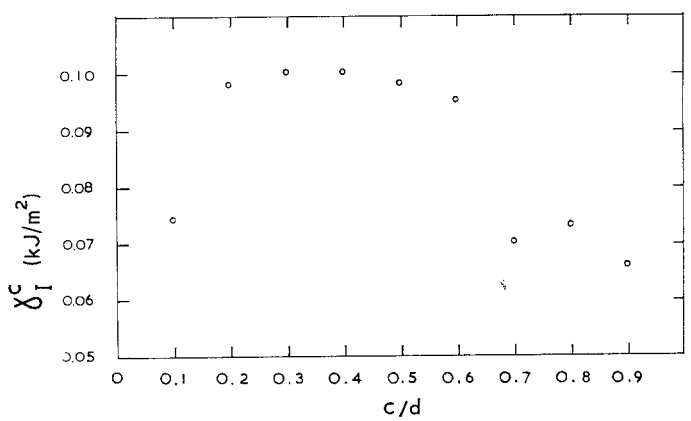

Figure 6 The values of fracture surface energy of initiation ($\gamma^e{}_I$) of a composite of $V_f = 0.52$ as a function of c/d.

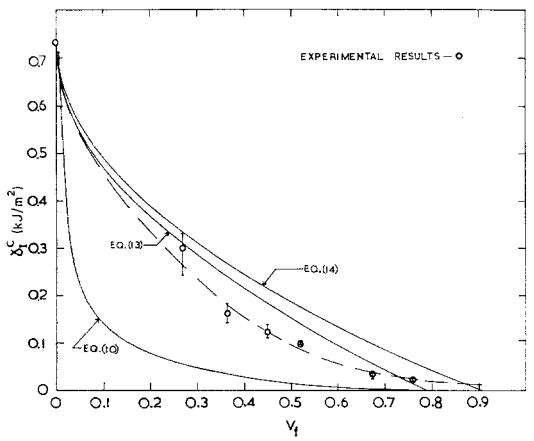

Figure 7 The experimental values of fracture surface energy of initiation as a function of V_f, compared with various theoretical relations.

of fracture, which itself depends on V_f and on the arrangement of the fibres in the matrix (random, hexagonal, square). From energy consideration the following applies:

$$\gamma_I{}^c A = \gamma_I{}^m A_m + \gamma_I{}^i A_i \quad (11)$$

where A_m and A_i are the matrix and the interface area respectively.

$$\gamma_I{}^c = \gamma_I{}^m \frac{A_m}{A} + \gamma_I{}^i \frac{A_i}{A} \quad (12)$$

By analogy to Section 3 and Equations 2 and 6 we obtain for a square array that

$$\gamma_I{}^c = \gamma_I{}^m [1 - \sqrt{(4V_f/\pi)}] + \gamma_I{}^i [\sqrt{(4V_f/\pi)}] \quad (13)$$

and for hexagonal array

$$\gamma_I{}^c = \gamma_I{}^m [1 - \sqrt{(2\sqrt{3}V_f/\pi)}] + \gamma_I{}^i [\sqrt{(2\sqrt{3}V_f/\pi)}] \quad (14)$$

Equations 13 and 14 are shown in Fig. 7 for $\gamma_I{}^m = 0.73$ kJ/m² and $\gamma_I{}^i = 0$.

By extrapolating the experimental results to $V_f = 0.906$ we find that $\gamma_I{}^i \approx 0.015$ kJ/m².

5. The average fracture surface energy, $\gamma_F{}^c$

5.1. Determination of $\gamma_F{}^c$

When a specimen fractures catastrophically, a curve of the type shown in Fig. 2a is recorded on the Instron. Controlled fracture leads to curves of the type shown in Figs. 2b and c [16]. In this case, all the elastic strain energy stored in the specimen during the testing and all the energy stored in the Instron machine, are converted into fracture surface energy. No losses, e.g. conversion into kinetic energy are incurred. In this situation, the area under the curve is related to the total work required to fracture the specimen completely [17].

Therefore:

$$\gamma_F{}^c = \frac{U}{2b(d-c)} \quad (15)$$

$\gamma_F{}^c$ was calculated for all composite specimens of every depth of cut. The results are summarized in Table III. Most of the $\gamma_F{}^c$ values show a consistent variation with c/d. The average over the range of $0.2 \leqslant c/d \leqslant 0.6$ was taken as the final value of $\gamma_F{}^c$ for every c/d value. All specimens of the pure matrix exhibited catastrophic fracture. The energy, as measured by the area under the fracture curve was, therefore, higher than the real value. In specimens with deep cuts the fracture process became progressively less catastrophic and the values of U for these specimens were close to the real value. The final value of $\gamma_F{}^m$ was determined by extrapolating the results of each set of specimens, with c/d values ranging from 0.1 to 0.9 to the point $c/d = 1$. All the sets gave an average of 0.3 kJ/m². The final results are shown in Fig. 8.

TABLE III $\gamma_F{}^c$ values of the composites

V_f	0.27	0.37	0.45	0.52	0.67	0.76
c/d	$\gamma_F{}^c$ (10^2 J/m²)					
0.1	4.4	4.7	5.2	2.4	1.9	1.2
0.2	3.4	3.2	3.1	2.1	1.4	0.91
0.3	3.3	3.7	3.0	2.1	1.6	0.85
0.4	3.2	3.5	3.6	1.8	1.2	0.66
0.5	3.5	2.6	2.0	1.7	0.93	0.61
0.6	3.0	3.1	2.6	1.6	0.82	0.54
0.7	2.7	2.0	1.8	1.2	0.53	0.41
0.8	3.2	1.7	1.4	1.3	0.62	0.29
0.9	2.4	1.8	1.5	0.70	0.64	—

5.2. $\gamma_F{}^c$ as a function of V_f

For the purpose of determining $\gamma_F{}^c$ as a function of V_f it is possible that the same considerations, used for the determination of a similar function of $\gamma_I{}^c$ apply. As scanning electron microscope studies of the fracture face prove that fibre breakage does take place during the complete process, a third term must be added to the equation for $\gamma_F{}^c$. By analogy to Equation 12 we can write:

$$\gamma_F{}^c = \gamma_F{}^m \frac{A_m}{A} + \gamma_F{}^i \frac{A_i}{A} + \gamma_F{}^f \frac{A_f}{A} \quad (16)$$

where A_f is the fibre surface area and A_f/A is

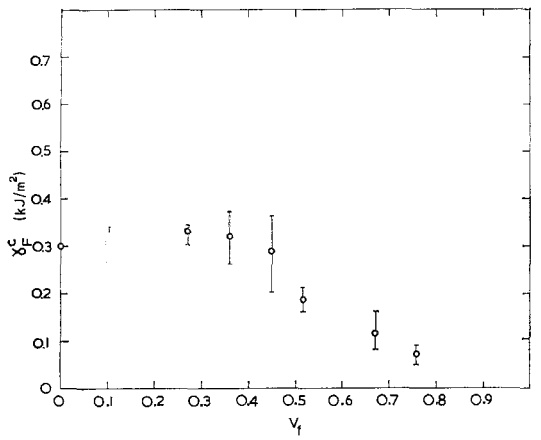

Figure 8 The experimental values of fracture surface energy of the complete process $\gamma_F{}^c$ as a function of V_f.

the fibre area fraction. While it is reasonable to assume that A_m/A and A_i/A have the same forms as in Equations 13 or 14, A_f/A is determined by the probability of fibre breakage during the process. This probability itself depends on various factors such as V_f and the degree of misalignment of the fibres.

In order to evaluate the contribution of the fibre breakage to $\gamma_F{}^c$ a determination of $\gamma_F{}^f$ was carried out by measuring the tensile energy, required to completely fracture a roving of the glass fibres. A typical load-deflection curve is shown in Fig. 9. The area under the curve is equivalent to the total tensile energy. The value

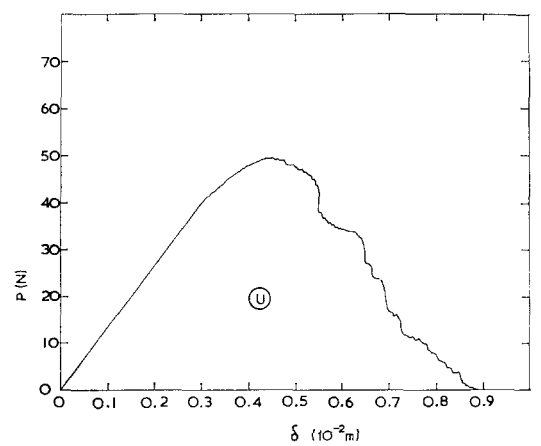

Figure 9 A typical load deflection curve for a glass-fibre roving. U is the energy required to completely fracture the roving.

found for rovings containing 408 fibres of 7.6×10^{-6}m radius was 0.23 J.

By substituting this energy value into the equation $\gamma_F{}^f = U/2A$, $\gamma_F{}^f$ was found to be 1.6 MJ/m². $\gamma_F{}^f$ is thus some four orders of magnitude greater than $\gamma_F{}^m$. Therefore, even if

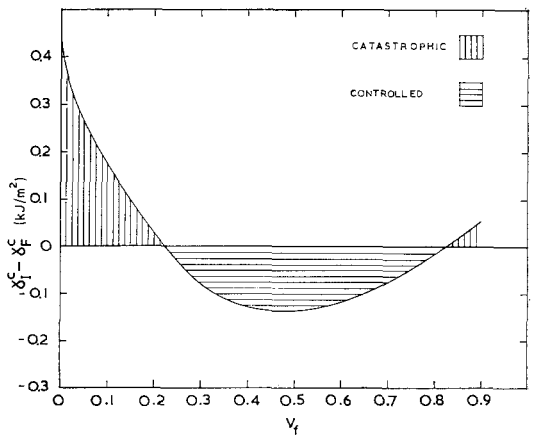

Figure 10 ($\gamma_I{}^c - \gamma_F{}^c$) as a function of the volume fraction of the fibres, and the ranges of catastrophic and controlled fracture processes.

the probability of fibre breakage is very low, the contribution of this process to the total average surface fracture energy is still dominant. It is obvious that the maximum contribution of $\gamma_F{}^f$ to $\gamma_F{}^c$ occurs for V_f values of about 0.45. By neglecting the contribution of $\gamma_F{}^m$ and $\gamma_F{}^i$ at this V_f value we find, that the approximate value of the fibre area fraction, A_f/A is 10^{-4}.

6. The nature of the transverse fracture process

By comparing the fracture curves of two composites of different V_f values (Figs. 2b and c), it is possible to see that there is a change in the degree of control of the process with V_f. It is clear that the nature of the transverse fracture process is governed by the relation of $\gamma_I{}^c$ to $\gamma_F{}^c$. For $\gamma_I{}^c - \gamma_F{}^c > 0$ we expect a catastrophic process and for $\gamma_I{}^c - \gamma_F{}^c < 0$ a controlled process is observed. The magnitude of the absolute value of $\gamma_I{}^c - \gamma_F{}^c$, determines the degree of control. Fig. 10 shows the ranges of controlled and catastrophic processes.

The fact that the probability of fibre breakage and the contribution of $\gamma_F{}^f$ to the value of $\gamma_F{}^c$

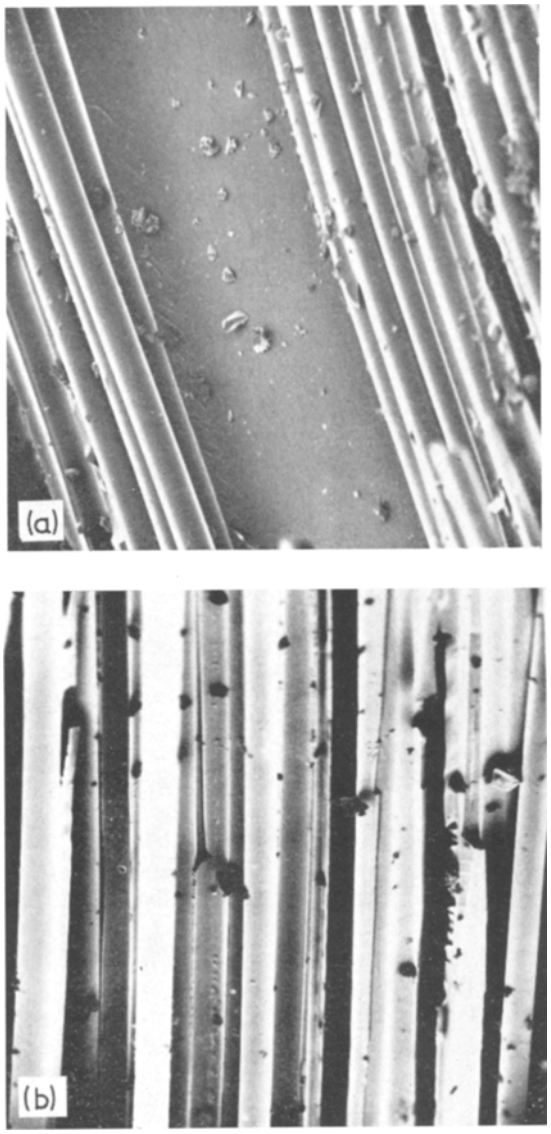

Figure 11 Scanning electron micrographs of transverse fracture faces (× 280). (a) V_f = 0.27, wide zone of fractured matrix between the fibre layers. (b) V_f = 0.52, narrow zones of matrix between the fibre layers.

are the crucial factors in determining the nature of the process are further supported by scanning electron microscope examinations of fracture faces. Fig. 11a shows a micrograph of the fracture face of a low V_f composite. It is obvious that the wide matrix zones between the fibre layers show brittle fracture without any plastic deformation. Figs. 11a and b shows that both for low and high V_f values the fibres separate completely from the matrix. But, in spite of the fact that the fracture develops parallel to the fibres it is possible to find broken fibres in both fracture faces. It also may be concluded that the transverse fracture process is composed of two simultaneous processes: one which is concerned with the matrix only and is catastrophic, and the other which concerns the fibres and the fibre-matrix interface which is a controlled fracture process. The nature of the overall process is solely determined by V_f.

References

1. S. P. PROSEN, *ASTM STP* 460 (1969) 5.
2. R. J. SANFORD and F. R. STONESIFER, *J. Comp. Mater.* **5** (1971) 241.
3. R. W. DAVIDGE and G. TAPPIN, *J. Mater. Sci.* **3** (1968) 165.
4. A. A. GRIFFITH, *Phil. Trans. R. Soc.* **A-221** (1921) 163.
5. E. SRAWLEY and F. BROWN, *ASTM STP* **381** (1964).
6. G. A. COOPER and A. KELLY, *ibid* **452** (1969) 90.
7. W. W. GERBERICH, *J. Mech. Phys. Solids* **19** (1971) 71.
8. F. J. MCGARRY, "Fundamental Aspects of Fibre Reinforced Plastic Composites". Eds. R. T. Schwartz and H. S. Schwartz (John Wiley, New York, 1968) p. 63.
9. G. R. IRWIN, NRL Report 5486 (July 1960).
10. H. T. CORTEN, "Fundamental Aspects of Fibre Reinforced Plastic Composites". Eds. R. T. Schwartz and H. S. Schwartz (John Wiley, New York, 1968) p. 89.
11. W. F. BROWN and J. E. SRAWLEY, *ASTM STP* **410** (1967).
12. B. GROSS and J. E. SRAWLEY, NASA TN-2603 (1965).
13. R. W. DAVIDGE and A. G. EVANS, *Mater. Sci. Eng.* **6** (1970) 281.
14. G. R. IRWIN, University of Illinois TAM Report 213 (1962).
15. H. WINNE and B. M. WUNDT, *Trans. ASME* **80** (1958) 1643.
16. J. NAKAYAMA, *Jap. J. Appl. Phys.* **7** (1964) 422.
17. H. G. TATTERSALL and G. TAPPIN, *J. Mater. Sci.* **1** (1966) 296.

Received 10 December 1971 and accepted 19 May 1972.